Supporting Information

Porous yet densely packed metal-organic frameworks (MOFs) toward ultrastable oxygen evolution at practical current densities

Haiming Wang[a,b], Ming Li,[a] Jingjing Duan[a], Sheng Chen[*a]

[a]Key Laboratory for Soft Chemistry and Functional Materials (Ministry of Education), School of Chemical Engineering, School of Energy and Power Engineering, Nanjing University of Science and Technology, Nanjing, Jiangsu 210094, China.
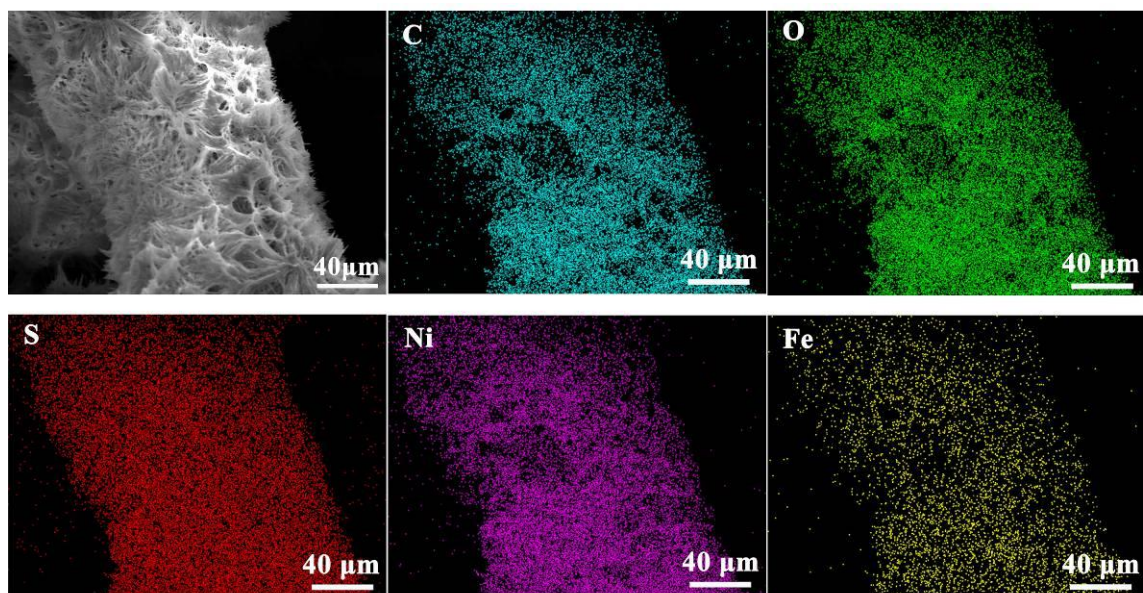
[b]College of Mechanical and Electronic Engineering, Tarim University, Alaer, Xinjiang 843300, China.

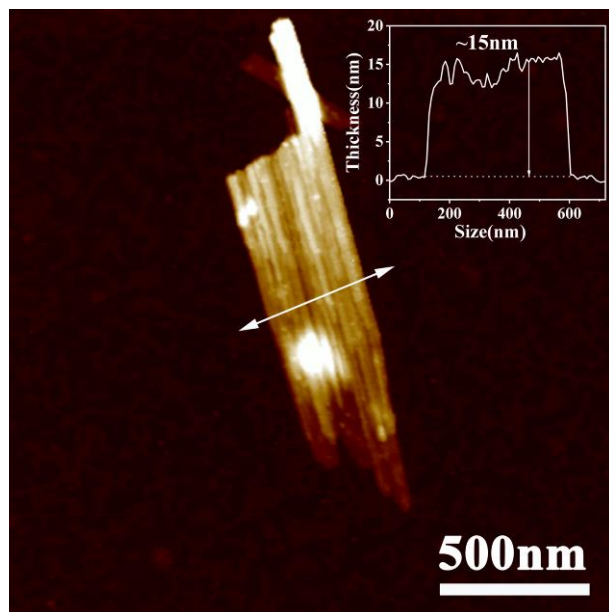*Corresponding e-mail: sheng.chen@njust.edu.cn (S.C.)
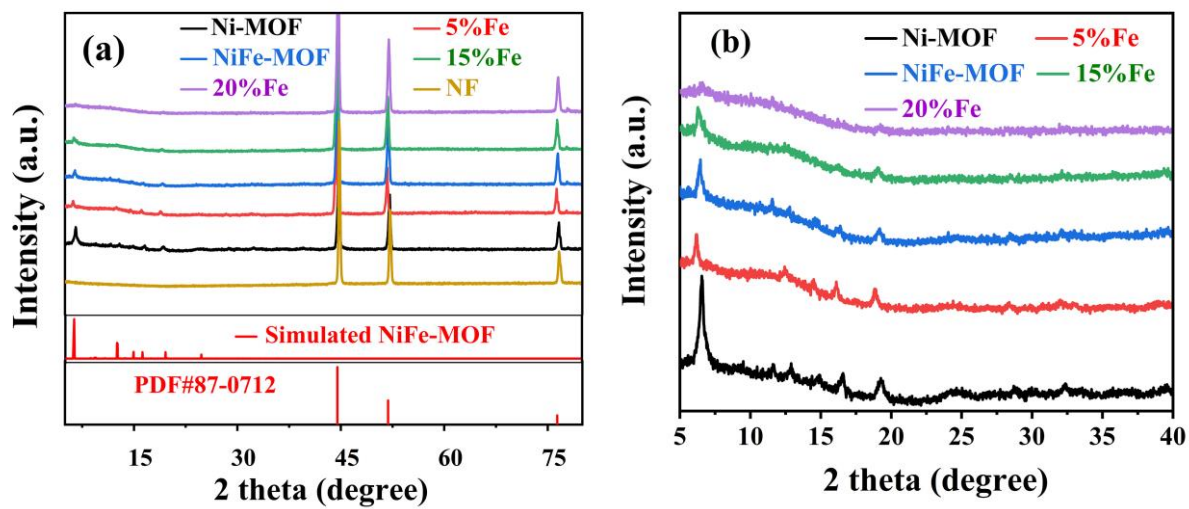
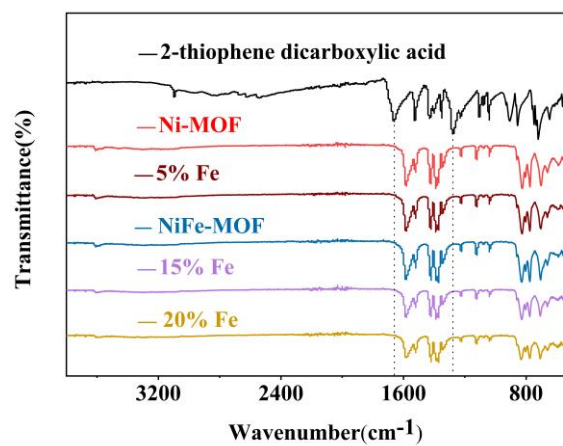**Fig. S1.** XRD patterns of NiFe-MOFs with different Fe wt%.

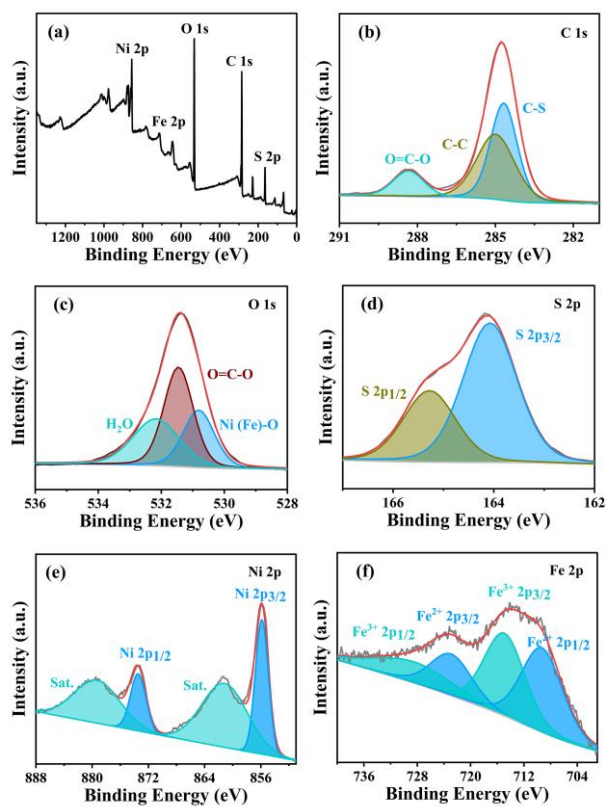(a)full spectrum, (b)partially amplified spectrum.

Fig. S2. SEM elemental mappings of NiFe-MOF.

Fig. S3. AFM image and corresponding height profile of NiFe-MOF.
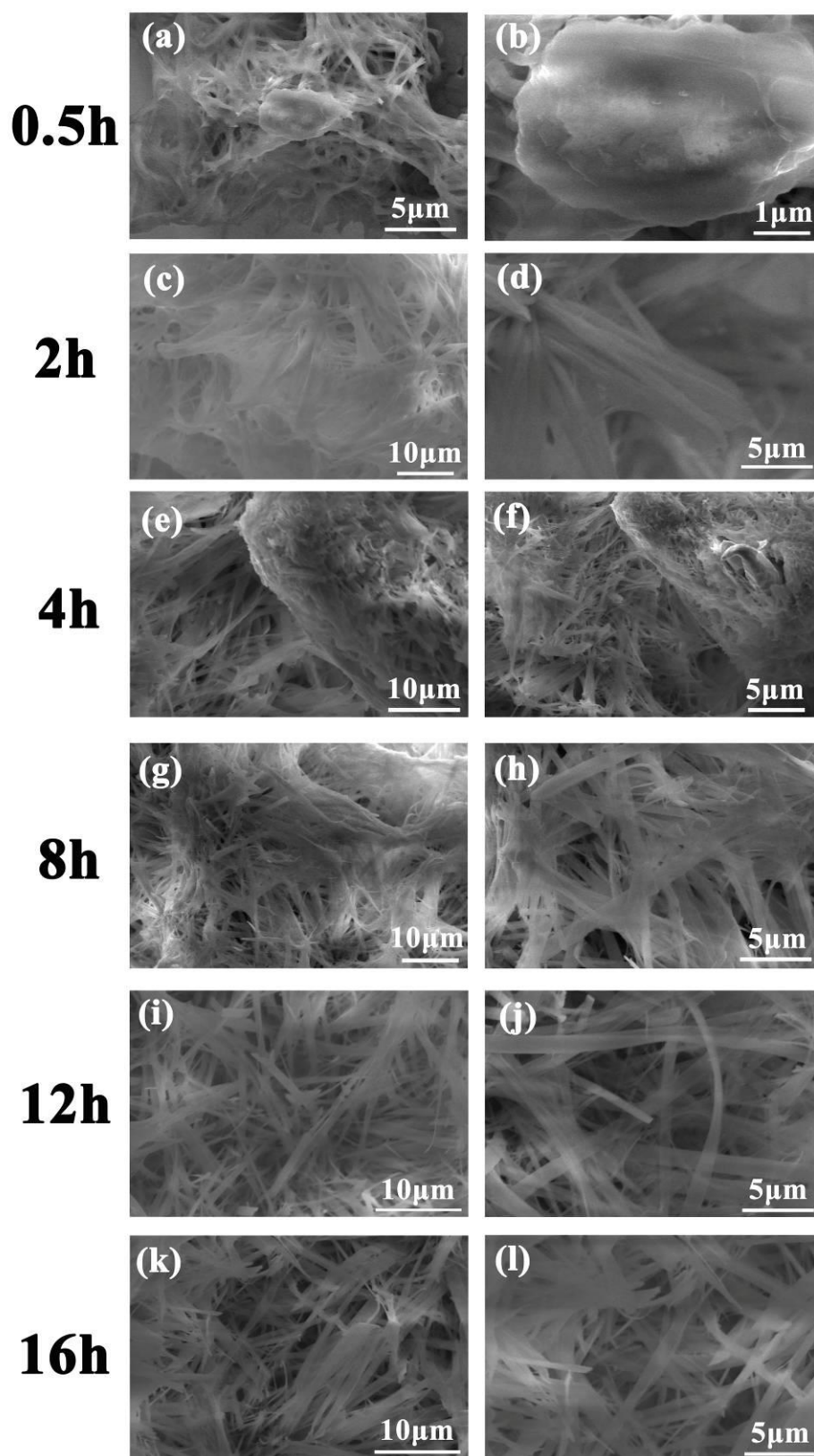
Fig. S4. FTIR spectra of NiFe-MOFs with different Fe wt%.

Fig. S5.XPS spectra of NiFe-MOF.

(a) Survey scan of NiFe-MOF, (b) C 1s, (c) O 1s, (d) S 2p, (e) Ni 2p, and (f) Fe 2p.

Fig. S6. SEM images of the reaction intermediates for forming NiFe-MOFs at different reaction durations. (a-b) 0.5 h, (c-d)2 h, (e-f) 4 h, (g-h) 8 h, (i-j) 12 h, (k-l)16 h

7
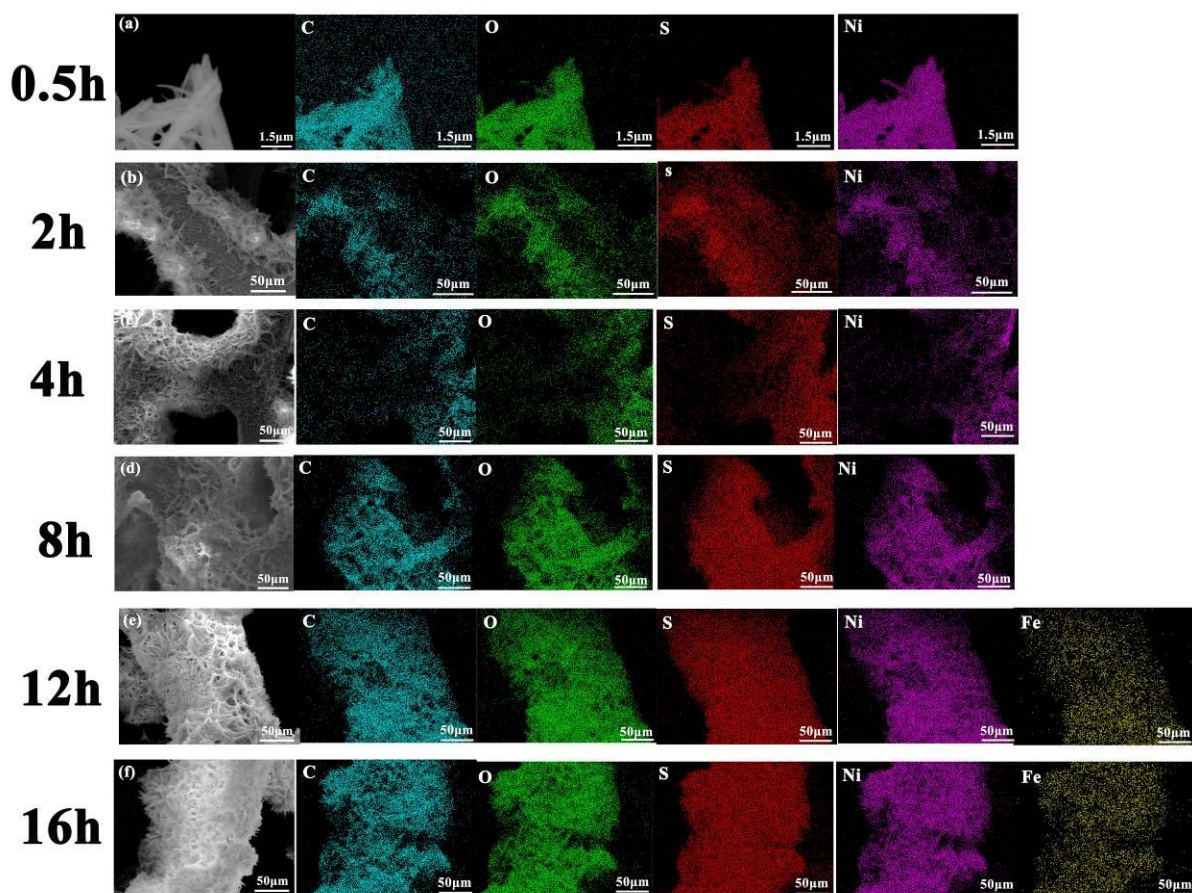
Fig. S7. SEM elemental mappings of the reaction intermediates for forming NiFe-MOF at different reaction durations.(a-b) 0.5 h, (c-d)2 h, (e-f) 4 h, (g-h) 8 h, (i-j) 12 h, (k-l) 16 h
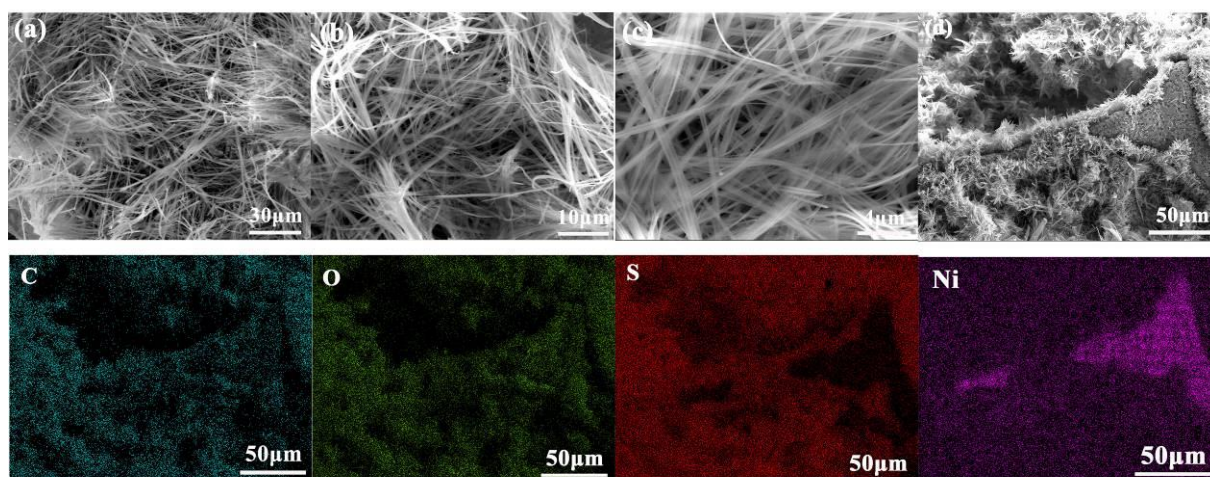
Fig. S8. SEM images and elemental mappings of Ni-MOF.
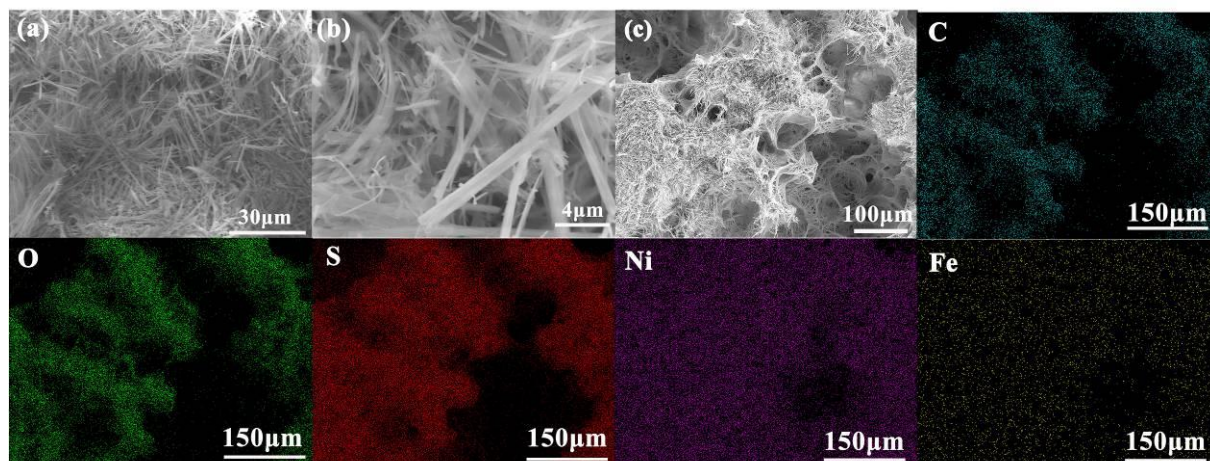
Fig.S9. SEM images and elemental mappings of NiFe-MOF (5% Fe).
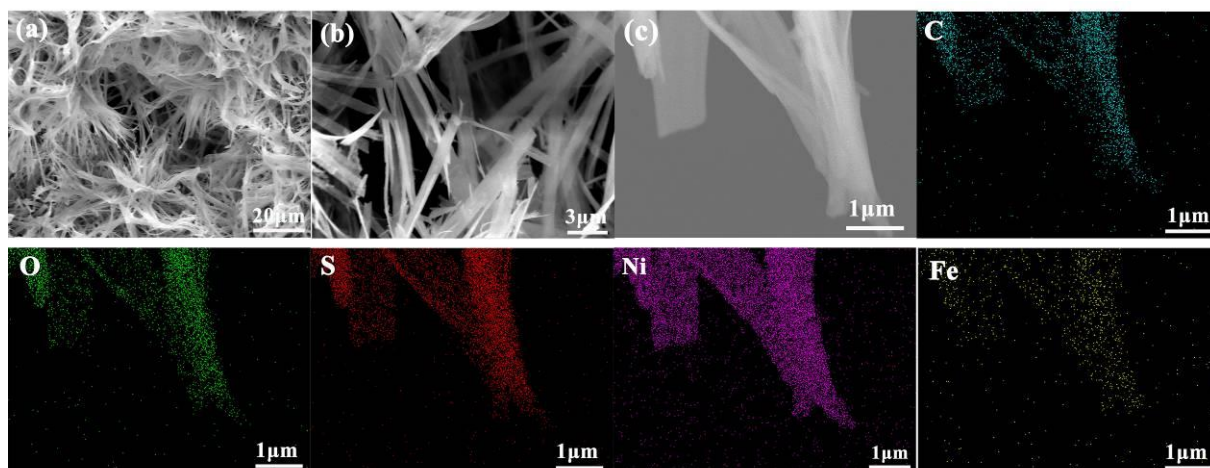
Fig. S10. SEM images and elemental mappings of NiFe-MOF (15% Fe).
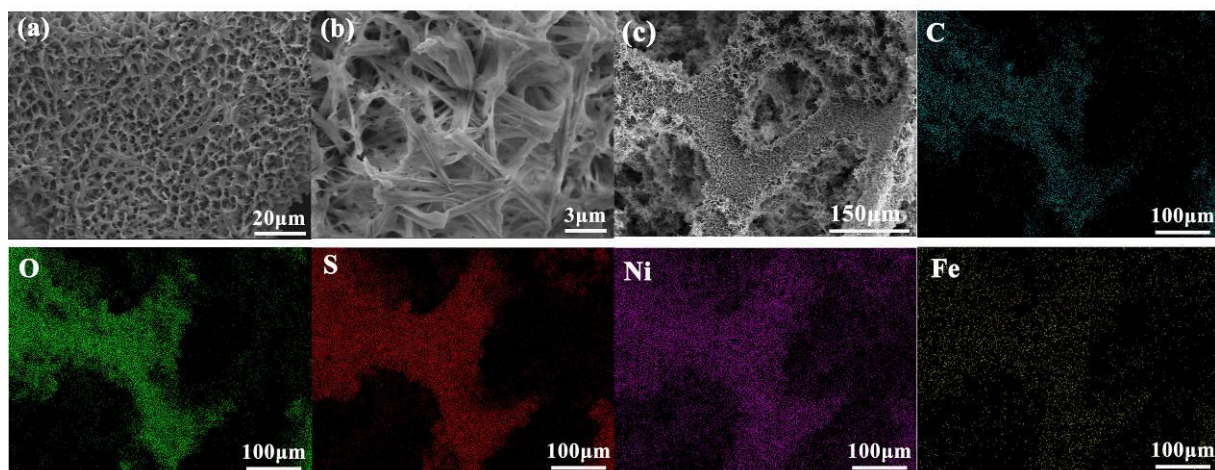
Fig. S11. SEM images and elemental mappings of NiFe-MOF (20% Fe).
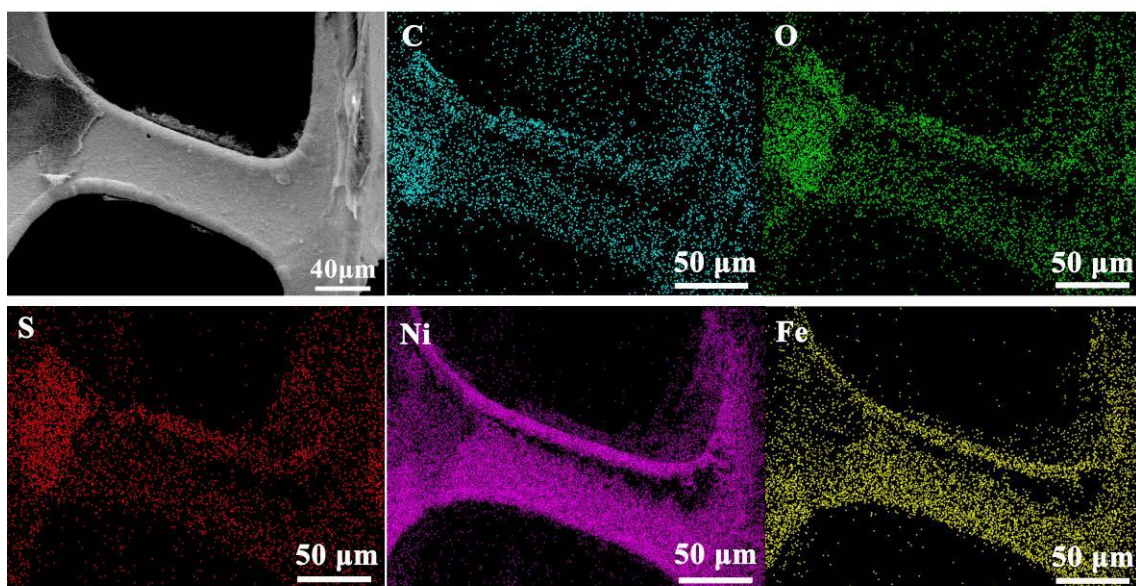
Fig.S12. SEM images and elemental mappings of NiFe-MOF-1.
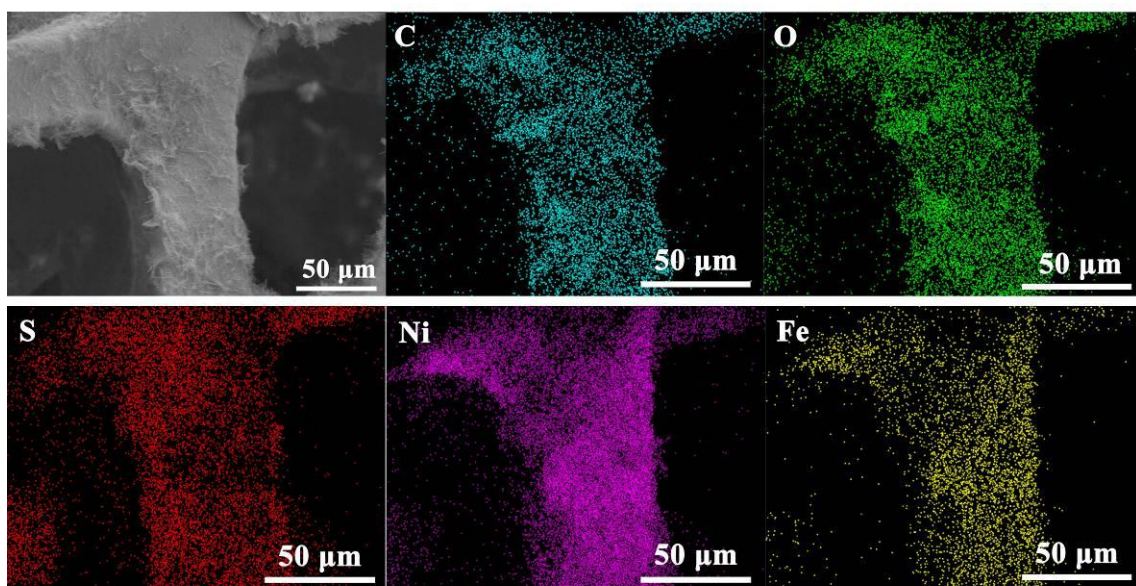
Fig. S13. SEM images and elemental mappings of NiFe-MOF-3.
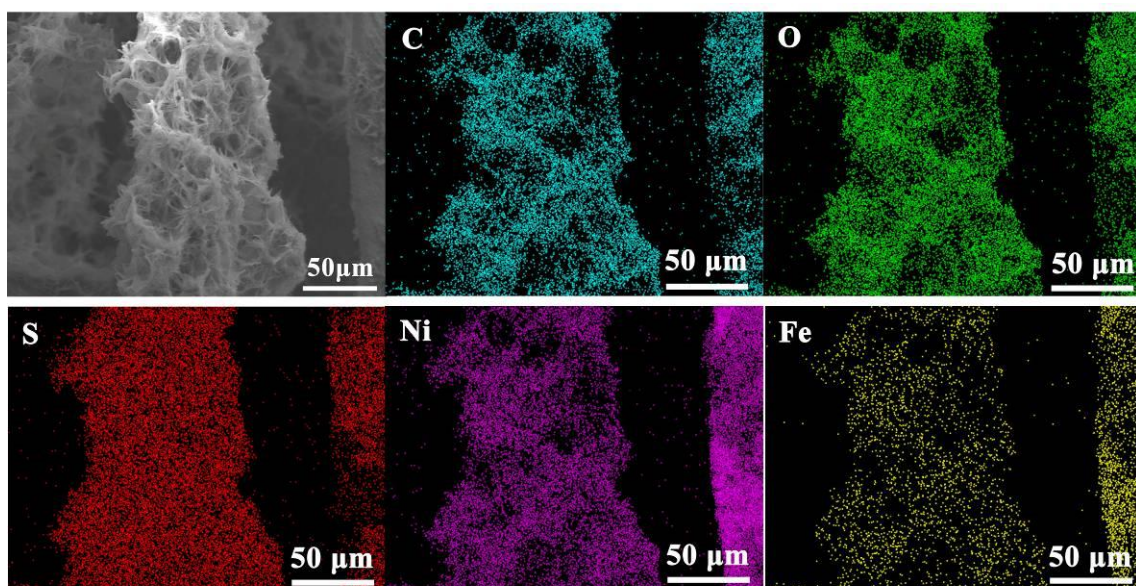
Fig. S14. SEM images and elemental mappings of NiFe-MOF-6.
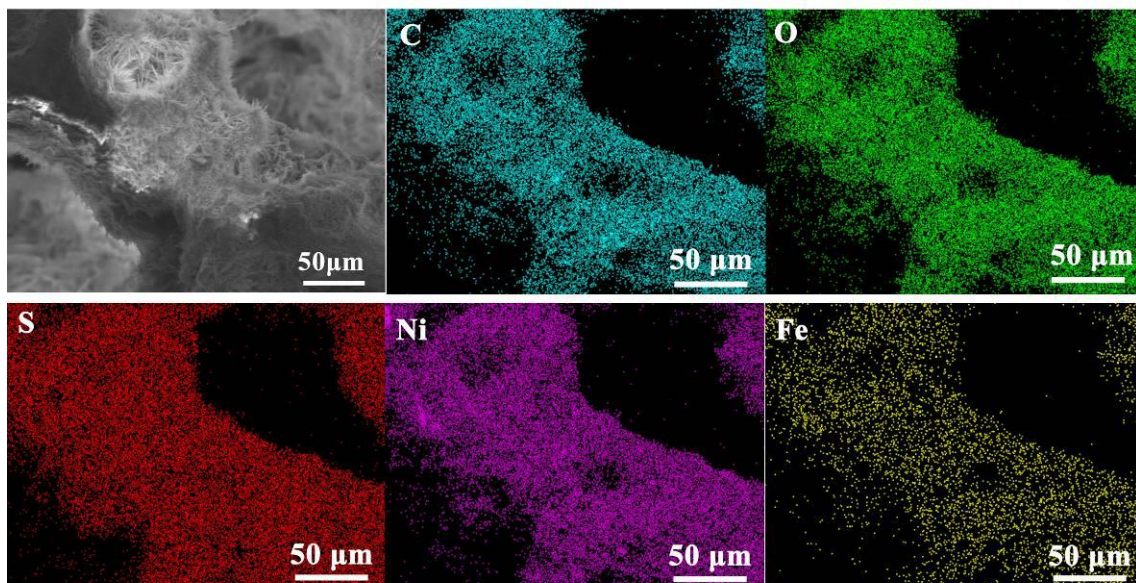
Fig. S15. SEM images and elemental mappings of NiFe-MOF-12.
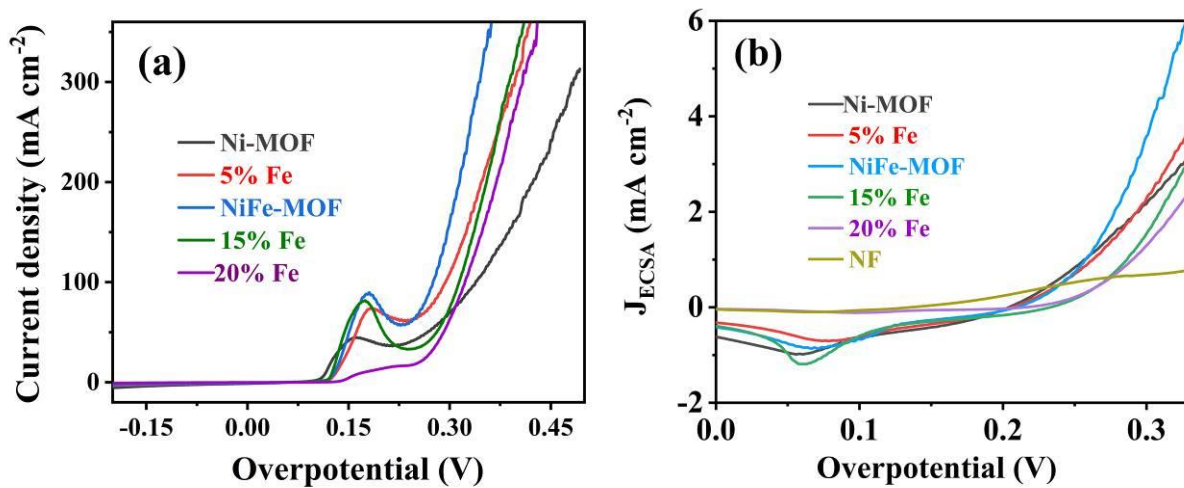
Fig. S16. LSV curves of NiFe-MOFs with different Fe wt%.

(a) LSV curves recorded by sweeping from low to high potentials (positive sweep), (b) LSV curves normalized by ECSA of different samples of Figs.2a (reverse sweep).
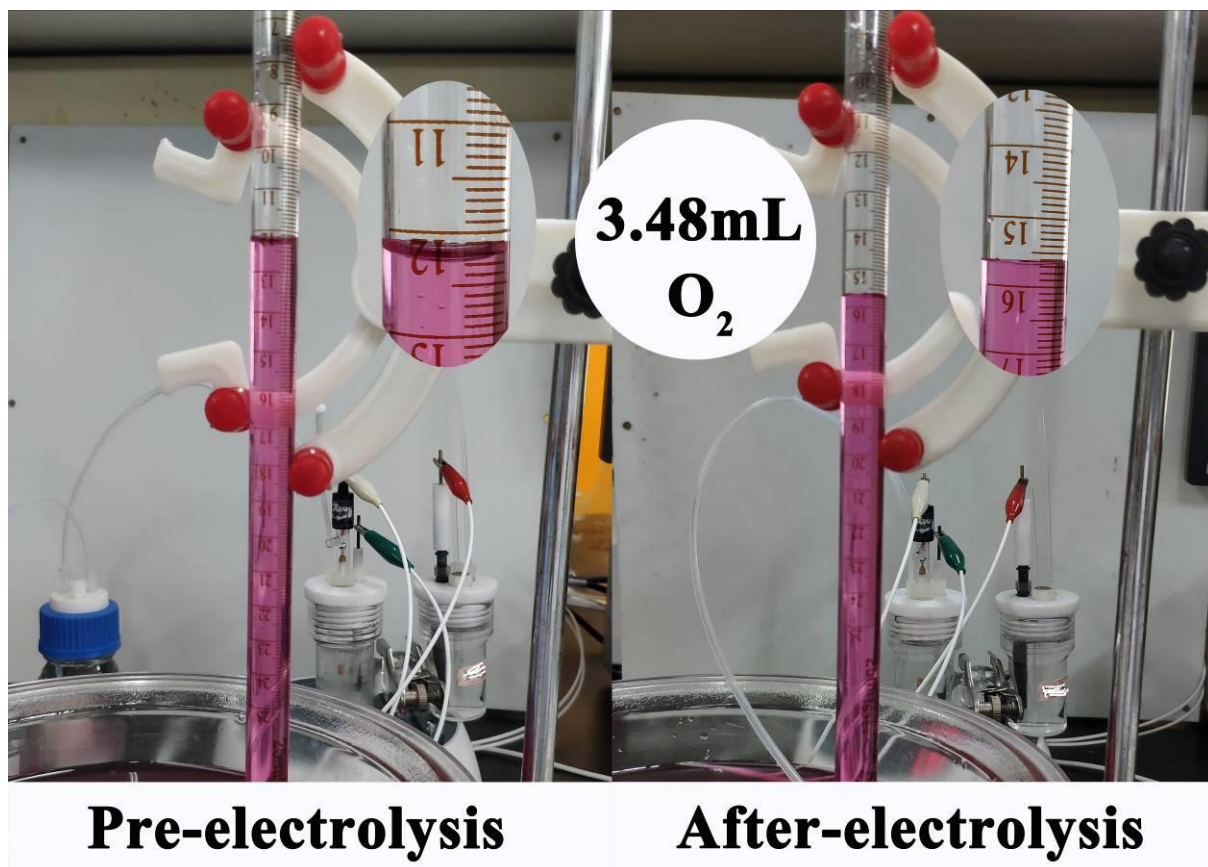
Fig. S17. Digital photograph of the equipment for measuring the volume of as-produced O_2 from oxygen evolution.
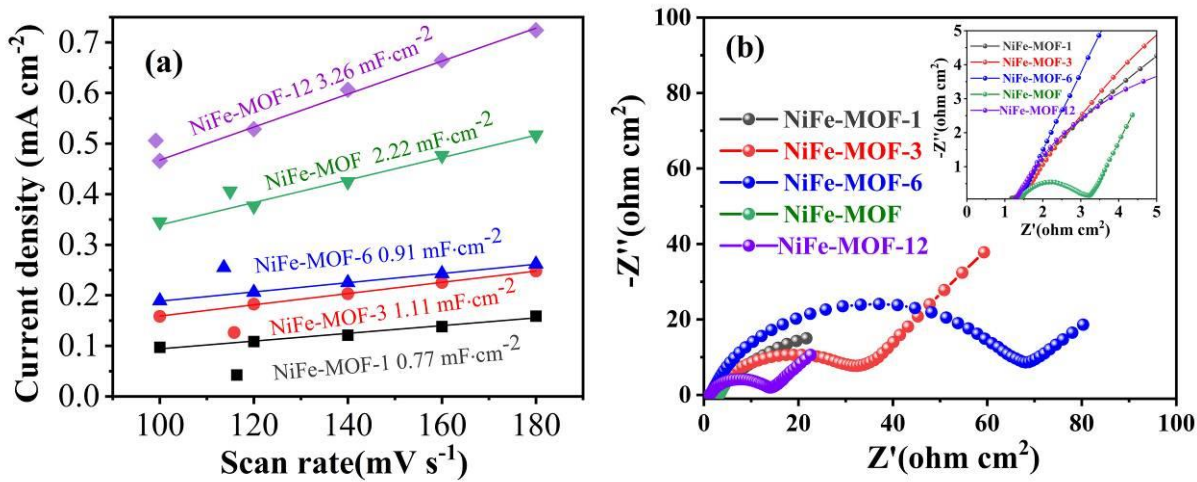
Fig. S18. (a) C_{dl} and (b)Nyquist plots of NiFe-MOF with different average mass loadings.
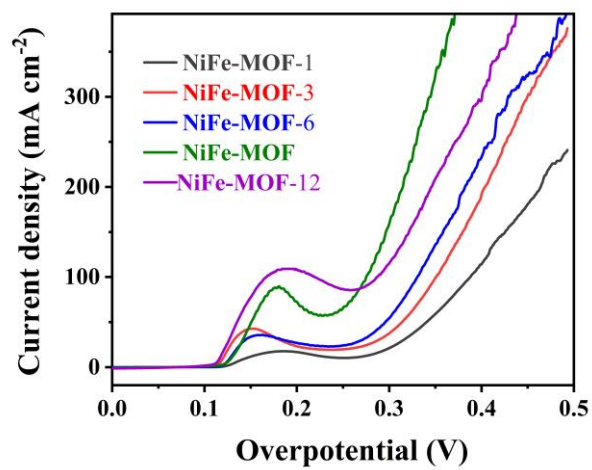
Fig. S19. LSV curves of NiFe-MOF with different average mass loadings(positive sweep).
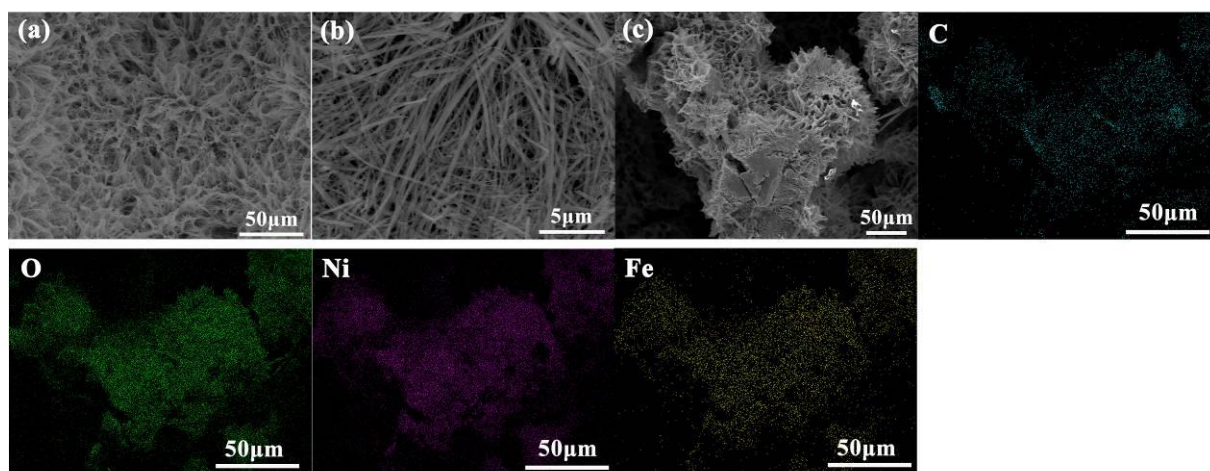
Fig. S20. SEM images and elemental mappings of NiFe-MOF after 666 h-electrocatalytic
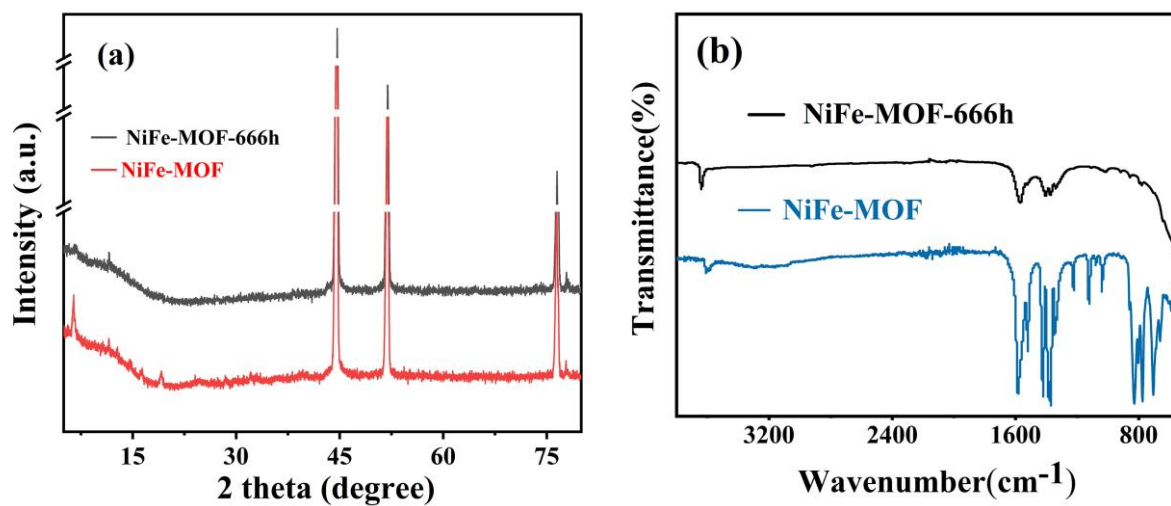
stability test.

Fig. S21. XRD patterns (a) and FTIR spectra (b) of NiFe-MOF before and 666h electrocatalytic stability test.
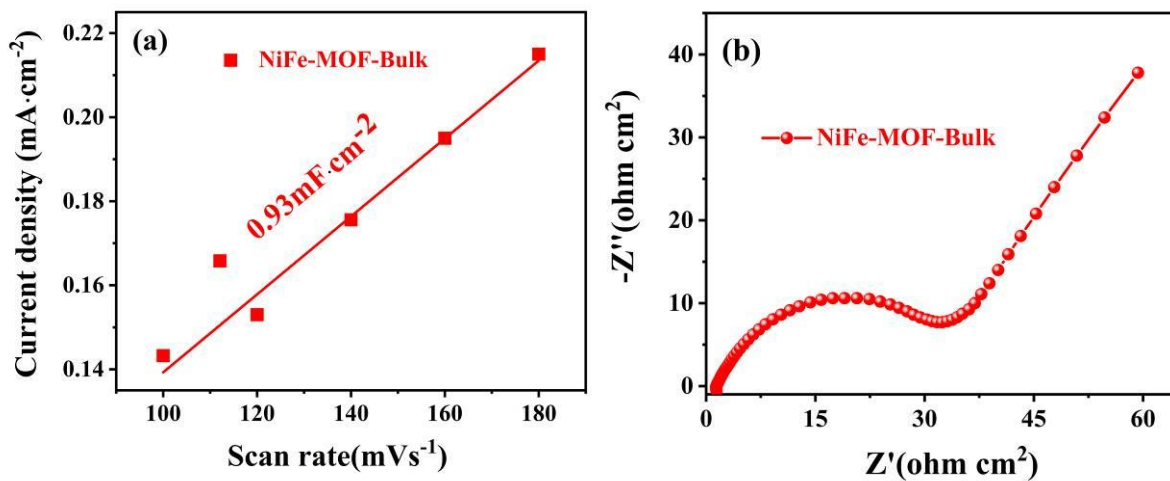
Fig. S22. (a) C_{dl} and (b) Nyquist plots of Bulk NiFe-MOF.
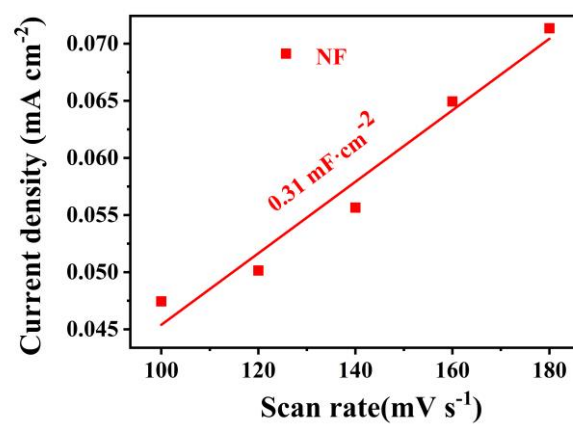
Fig. S23. C_{dl} of nickel foam (NF)
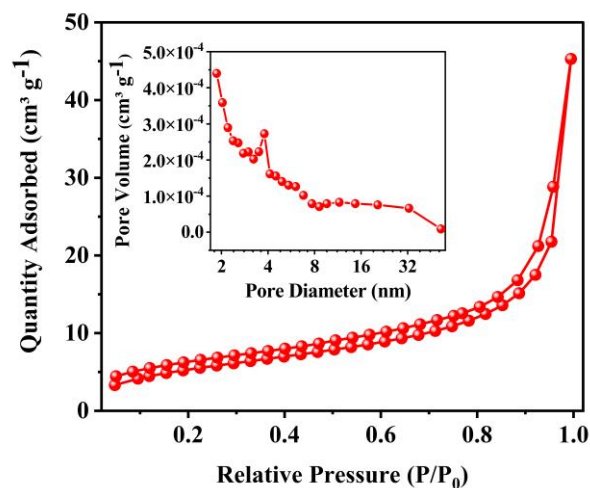
Fig. S24. N$_2$ adsorption−desorption isotherms with the pore size distribution curves by the BJH method (inset) of NiFe-MOF

Supplementary **n**ote: The Brunauer−Emmett−Teller (BET) gas-sorption measurements demonstrate that the NiFe-MOF material has a type III isotherm with a distinct hysteresis loop at relative pressures (P/P$_0$) of 0.05−1, the corresponding BET specific surface area is about 20 m^2 g^{-1}. Further, corresponding pore size distribution shows the presence of mesopores of 3.8 nm.

.

Table S1. ICP-MS analysis of NiFe-MOF sample.

No.		Content (wt.%)		
		Ni	Fe	Total content
1	NiFe-MOF	33.97%	1.55%	34.52%

Table S2. Overpotentials of NiFe-MOF and other comparison samples.

No.	Sample name	Overpotential (mV)			
		10 mA cm^{-2}	100 mA cm^{-2}	200 mA cm^{-2}	300 mA cm^{-2}
1	Ni-MOF	229	350	427	480
2	NiFe-MOF	226	278	305	327
3	Bulk	324		463@50mA cm^{-2}	
4	NF	372		494@50mA cm^{-2}	
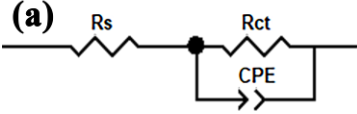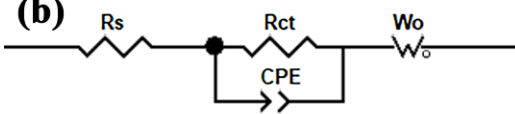
Table S3. EIS simulation of NiFe-MOF with different Fe%.

		Rs	Rct	Wo
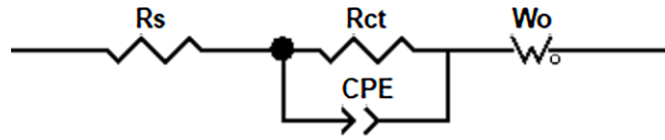
Model:

No.	Sample name	R_S/Ω	R_{ct}/Ω
1	Ni-MOF	1.285	7.508
2	NiFe-MOF-5%Fe	1.35	6.883
3	NiFe-MOF	1.384	1.596
4	NiFe-MOF-15%Fe	1.328	18.66
5	NiFe-MOF-20%Fe	1.118	47.04
6	NiFe-MOF-Bulk	1.39	30.9

Table S4. EIS simulation of NiFe-MOF with different mass loadings.

No.	Sample name	R_S/Ω	Rct/Ω	Model
1	NiFe-MOF-1	1.197	58.94	a
2	NiFe-MOF-3	1.381	30.91	b
3	NiFe-MOF-6	1.412	63.99	b
4	NiFe-MOF	1.386	1.606	b
5	NiFe-MOF-12	1.274	12.3	b

note：NiFe-MOF-1,NiFe-MOF-3, NiFe-MOF-6, NiFe-MOF, and NiFe-MOF-12 mean the mass loading is ~1. 3,6,10,12 mg cm^{-2} respectively, please see more in Table S5-S9.

Table S5. Average mass loadings of NiFe-MOF-1 on NF substrate.

Measured No.	m(NF)/mg	m(NiFe-MOF)/ mg	Area/cm^{-2}	Mass loading/mg cm^{-2}
1	215.99	223.36	6.68	1.10
2	211.41	218.93	6.76	1.13
3	218.74	226.03	6.66	1.09
4	217.08	224.99	6.92	1.14
5	216.08	223.61	6.97	1.08
average				1.11

Table S6. Average mass loadings of NiFe-MOF-3 on NF substrate.

Measured No.	m(NF)/mg	m(NiFe-MOF)/mg	Area/cm^{-2}	Mass loading/mg cm^{-2}
1	215.89	237.23	6.71	3.18
2	212.43	233.65	6.78	3.13
3	217.84	238.8	6.76	3.1
4	217.38	239.13	6.97	3.12
5	216.56	238.41	7.07	3.09
average				3.12

Table S7. Average mass loadings of NiFe-MOF-6 on NF substrate.

Measured No.	m(NF)/mg	m(NiFe-MOF)/mg	Area/cm^{-2}	Mass loading/mg cm^{-2}
1	216.92	259.58	6.88	6.20
2	213.53	218.93	6.87	6.21
3	218.24	256.19	6.67	6.08
4	217.45	261.4	6.90	6.37
5	216.57	267.3	6.99	6.25
average				6.22

Table S8. Average mass loadings of NiFe-MOF on NF substrate.

Measured No.	m(NF)/mg	m(NiFe-MOF)/ mg	Area/cm^{-2}	Mass loading/mg cm^{-2}
1	216.09	285.68	6.89	10.10
2	213.42	281.36	6.87	9.89
3	217.84	286.17	6.93	9.86
4	286.36	224.99	7.02	9.94
5	216.48	287.04	7.07	9.98
average				9.95

Table S9. Average mass loadings of NiFe-MOF-12 on NF substrate.

Measured No.	m(NF)/mg	m(NiFe-MOF)/ mg	Area/cm^{-2}	Mass loading/mg cm^{-2}
1	215.78	300.24	6.98	12.10
2	211.87	294.07	6.89	11.93
3	301.08	226.03	6.87	12.09
4	217.34	300.92	6.89	12.13
5	300.81	223.61	6.98	12.07
average				12.06

Table S10. Comparison of alkaline OER activities for NiFe-MOF with recently reported MOF based electrocatalysts.

Catalysts	η_{10} (mV)	η_{50} (mV)	η_{100} (mV)	Electrolyte	Ref.
NiFe-MOF honeycombs	226	258	278	1 M KOH	**This work**
MOF/LDH	/	216	227	1 M KOH	1
MOF Fragments	203	/	238	1 M KOH	2
NiCoFe-MOF	257	/	/	1 M KOH	3
1-3D NiFe-MOF	223	/	263	1 M KOH	4
MOF/graphene	106	/	/	1 M KOH	5
HE MOF	/	254	/	1 M KOH	6
CoBDC–Fc	178	/	241	1 M KOH	7
NiCoFe-MOF	219	/	/	1 M KOH	8
NiYCe-MOF	245	/	/	1 M KOH	9
CoNi-MOF-NA	215	/	/	1 M KOH	10
Quasi-2D MOF	270	317	/	1 M KOH	11

Table S11. Comparison of alkaline OER stabilities for MOF based electrocatalysts.

Catalysts	h (10 mA cm^{-2})	h (100 mA cm^{-2})	h(500 mA cm^{-2})	Mass loading /mg cm^{-2}	Ref.
NiFe-MOF honeycombs	/	666h@98%	100h@97.1%	9.95	**This work**
MOF/LDH	/	100h@99%	100h@91% at 300 mA cm^{-2}	1.8	1
MOF Fragments	1080h@97%	/	/	/	2
NiCoFe-MOF	35h@96%	/	/	0.54	3
1-3D NiFe-MOF	/	70h@97%	/	/	4
MOF/graphene	150h@100%	/	/	13.82	5
HE MOF	100h@99%	5h@97%	5h@87%	0.76	6
CoBDC–Fc	/	80h@99%	/	2	7
NiCoFe-MOF	60h@93.3% at 0.3V	/	/	/	8
NiYCe-MOF	/	100h@94%	100h@90% at 200 mA cm^{-2}	13.5	9
CoNi-MOF-NA	300h@98.6%	20h@93.5%	/	2	10
Quasi-2D MOF	30h@99%at 20 mA cm^{-2}	300h@99% at 50 mA cm^{-2}	/	5.2	11
Lattice-strained NiFe MOFs	/	200h@97% at 200 mA cm^{-2}	/	2	12

Supporting References

1 Y. Wang, L. Yan, K. Dastafkan, C. Zhao, X. Zhao, Y. Xue, J. Huo, S. Li and Q. Zhai, Lattice matching growth of conductive hierarchical porous MOF/LDH heteronanotube arrays for highly efficient water oxidation, *Adv. Mater.*, 2021, **33**, 2006351.

2 W. H. Choi, K. H. Kim, H. Lee, J. W. Choi, D. G. Park, G. H. Kim, K. M. Choi and J. K. Kang, Metal-organic fragments with adhesive excipient and their utilization to stabilize multimetallic electrocatalysts for high activity and robust durability in oxygen evolution reaction, *Adv. Sci.*, 2021, **8**, 2100044.

3 Q. Qian, Y. Li, Y. Liu, L. Yu and G. Zhang, Ambient fast synthesis and active sites deciphering of hierarchical foam-like trimetal-organic framework nanostructures as a platform for highly efficient oxygen evolution electrocatalysis, *Adv. Sci.*, 2019, **31**, 1901139.

4 K. Yue, J. Liu, C. Xia, K. Zhan, P. Wang, X. Wang, Y. Yan and B. Y. Xia, Controllable synthesis of multidimensional carboxylic acid-based NiFe MOFs as efficient electrocatalysts for oxygen evolution, *Mater. Chem. Front.*, 2021, **5**, 7191-7198.

5 S. Lyu, C. Guo, J. Wang, Z. Li, B. Yang, L. Lei, L. Wang, J. Xiao, T. Zhang and Y. Hou, Exceptional catalytic activity of oxygen evolution reaction via two-dimensional graphene multilayer confined metal-organic frameworks, *Nat. Commun.*, 2022, **13**, 6171.

6 S. Xu, M. Li, H. Wang, Y. Sun, W. Liu, J. Duan and S. Chen, High-entropy metal-organic framework arrays boost oxygen evolution electrocatalysis, *J. Phys. Chem. C*, 2022, **126**, 14094-14102.

7 Z. Xue, K. Liu, Q. Liu, Y. Li, M. Li, C. Y. Su, N. Ogiwara, H. Kobayashi, H. Kitagawa, M. Liu and G. Li, Missing-linker metal-organic frameworks for oxygen evolution reaction, *Nat. Commun.*, 2019, **10**, 5048.

8 F. L. Li, Q. Shao, X. Huang and J. P. Lang, Nanoscale trimetallic metal-organic frameworks enable efficient oxygen evolution electrocatalysis, *Angew. Chem. Int. Ed. Engl.*, 2018, **57**, 1888-1892.

9 F. Li, M. Jiang, C. Lai, H. Xu, K. Zhang and Z. Jin, Yttrium- and cerium-codoped ultrathin metal-organic framework nanosheet arrays for high-efficiency electrocatalytic overall water splitting, *Nano Lett.*, 2022, **22**, 7238-7245.

10 L. Huang, G. Gao, H. Zhang, J. Chen, Y. Fang and S. Dong, Self-dissociation-assembly of ultrathin metal-organic framework nanosheet arrays for efficient oxygen evolution, *Nano Energy*, 2020, **68**, 104296.

11 C. P. Wang, H. Y. Liu, G. Bian, X. Gao, S. Zhao, Y. Kang, J. Zhu and X. H. Bu, Metal-layer assisted growth of ultralong quasi-2D MOF nanoarrays on arbitrary substrates for accelerated oxygen evolution, *Small*, 2019, **15**, 1906086.

12 W. Cheng, X. Zhao, H. Su, F. Tang, W. Che, H. Zhang and Q. Liu, Lattice-strained metal-organic-framework arrays for bifunctional oxygen electrocatalysis, *Nat. Energy*, 2019, **4**, 115-122.